

ON THE SIZES OF IONIZED BUBBLES AROUND GALAXIES DURING THE REIONIZATION EPOCH. THE SPECTRAL SHAPES OF THE LYMAN-ALPHA EMISSION FROM GALAXIES III.

MATTHEW J. HAYES¹ AND CLAUDIA SCARLATA²

¹Stockholm University, Department of Astronomy and Oskar Klein Centre for Cosmoparticle Physics, AlbaNova University Centre, SE-10691, Stockholm, Sweden.

²Minnesota Institute for Astrophysics, School of Physics and Astronomy, University of Minnesota, 316 Church Str. SE, Minneapolis, MN 55455, USA

(Received March 10, 2023; Revised XXX; Accepted March 7, 2023)

Submitted to ApJ

ABSTRACT

We develop a new method to determine the distance between a galaxy and a foreground screen of atomic hydrogen. In a partially neutral universe, and under the assumption of spherical symmetry, this equates to the radius of a ionized ‘bubble’ (R_{Bub}) surrounding the galaxy. The method requires an observed Ly α equivalent width, velocity offset from systemic, and an input Ly α profile for which we adopt scaled versions of the profiles observed in low- z galaxies. We demonstrate the technique in a sample of 21 galaxies at redshift $z > 6$, including six at $z = 7.2 - 10.6$ recently observed with JWST. Our model estimates the emergent Ly α properties, and the foreground distance to the absorbing IGM. We find that galaxies at $z > 7.5$ exist in smaller bubbles (~ 1 pMpc) than those at $z < 7$. With a relationship that is secure at better than 3σ , we empirically demonstrate the growth of ionized regions during the reionization epoch for the first time. We independently estimate the upper limit on the Strömgen radii (R_{Strom}), and derive the escape fraction of ionizing photons ($f_{\text{esc}}^{\text{LyC}}$) from the ratio of $R_{\text{Bub}}/R_{\text{Strom}}$, deriving a median value of 17% which on average can provide the photon budget necessary for reionization.

Keywords: cosmology: reionization – galaxies: evolution – galaxies: high-redshift – galaxies: intergalactic medium – galaxies: emission lines – radiative transfer

1. INTRODUCTION

Observations of Ly α emission from galaxies have long been known to fulfill a key role in charting the history of cosmic reionization (see [Dijkstra 2014](#), for a review). Because nebular Ly α emission can be redshifted from the systemic value (typically by a few hundred km s⁻¹) it can be detected through the damping wing of the Gunn-Peterson trough ([Miralda-Escudé & Rees 1998](#)), albeit with possibly-significant attenuation. This makes the population Ly α -emitting galaxies a very powerful tool to study the epoch of reionization (EoR), where a abundant Ly α -emitting galaxy population produces strong line emission just redward of systemic velocity.

Purely photometric Ly α measurements have been employed for EoR studies for almost two decades. The most common approaches so far have been to study flux deficit of Ly α compared with expectations. The first attempts performed differential comparison of the Ly α luminosity function (LF)

across redshifts (e.g. [Malhotra & Rhoads 2004](#); [Kashikawa et al. 2006](#)), although see [Dijkstra et al. \(2007\)](#) for further considerations. Developments of the technique study Ly α in comparison to the UV continuum flux, either as the ‘volumetric escape fraction’ ([Hayes et al. 2011](#); [Wold et al. 2017](#)) or an evolution of the equivalent with distribution ([Stark et al. 2011](#); [Schenker et al. 2014](#); [Cassata et al. 2015](#); [Arrabal Haro et al. 2018](#)). These methods, however, all rely up an ensemble of galaxies to derive one quantity, which is typically the average neutral fraction (\bar{x}_{HI}) at a given redshift (e.g. [Mason et al. 2018](#)). One cannot trivially derive higher order estimates of the reionization process, such as spatial variation, bubble size distribution, etc. For this kinematic/spectroscopic data are needed.

More nuanced estimates can be attained if the intrinsic Ly α properties of a galaxy are known: specifically comparisons of the observed Ly α EW and velocity profiles with their intrinsic values would lead directly to a measure of the distance between a galaxy and the foreground screen of absorbing H I. Little progress has been made because we need to know both the EW and velocity offset of emergent Ly α , which depend on stellar conditions and internal radiative transfer effects ([Ver-](#)

hamme et al. 2006; Dijkstra et al. 2006; Laursen et al. 2009). Moreover, without systemic redshifts we cannot even begin to estimate the velocity offset with respect to that of the IGM (simply distance in an expanding universe). Mason & Gronke (2020) provide the singular exception to this, attempting to circumvent the problem using a double-peaked Ly α -emitter and deriving a bubble radius of ≈ 0.7 pMpc in the $z = 6.6$ galaxy COLA1 (Matthee et al. 2018).

However this field is rapidly changing, and over recent years systemic redshifts have become available from other far ultraviolet emission lines like C III] $\lambda\lambda 1907, 1909\text{\AA}$ (Stark et al. 2015, 2017; Mainali et al. 2017) and infrared lines like [C II]158 μm (Pentericci et al. 2016; Carniani et al. 2017; Endsley et al. 2022). More recently, JWST has delivered the restframe optical emission lines to provide systemic redshifts and also even find Ly α emission at $z > 7.2$ (Tang et al. 2023; Saxena et al. 2023) and even almost $z \approx 11$ (Bunker et al. 2023). Thus, part of the requirement of having systemic redshifts and Ly α EWs and velocity offsets are now falling into place.

In this Paper we take advantage of the fact that Ly α EWs and velocity offsets are now being measured at $z > 6$ and 7. We study a sample of 21 galaxies at $z = 6 - 11$ with systemic redshifts and Ly α EWs and velocity shifts, which we present in Section 2. Their intrinsic Ly α profiles are not known, but using a large sample of low- z galaxies (Hayes et al. 2021, 2023) where IGM attenuation is negligible, we build realistic models for the Ly α that emerges from galaxies. Using the expected damping wing from a neutral universe, we build a model for the emergent Ly α observables, fitting the size of the ionized region and emergent Ly α EW in a hierarchical Bayesian framework. Thus, we empirically derive the distribution of the sizes of ionized bubbles that surround galaxies across most of the reionization timeline. This method is described in Section 3 and the results in Section 4. We present our concluding remarks in Section 5. Throughout we assume a cosmology of $\{H_0, \Omega_M, \Omega_\Lambda\} = \{70 \text{ km s}^{-1} \text{ Mpc}^{-1}, 0.3, 0.7\}$ and the cosmic baryon density.

2. THE GALAXY SAMPLE

We obtain the spectral measurements for 21 galaxies at $z > 6$. We first adopt the fifteen compiled by Endsley et al. (2022), searching the primary references to obtain uncertainties on Ly α EW and the velocity offset of the line ($\Delta v_{\text{red}}(\text{Ly}\alpha)$). We add recent JWST-observations of six more galaxies: four from the The Cosmic Evolution Early Release Science Survey (CEERS, Finkelstein et al. 2022) that have Ly α detections in Tang et al. (2023) at $z = 7.4 - 8.7$; and JADES targets GNz11 at $z = 10.6$ (Bunker et al. 2023) and GS-z7-LA at $z \approx 7.3$ (Saxena et al. 2023). The main properties of interest are Ly α EW, velocity offset of the red peak, systemic redshifts and

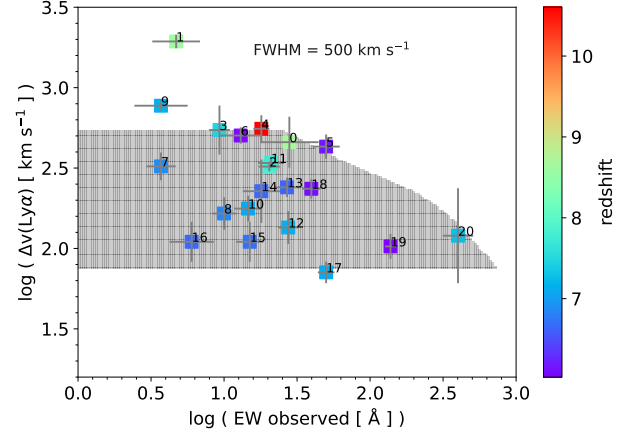


Figure 1. The Ly α observables of our sample. $\Delta v_{\text{red}}(\text{Ly}\alpha)$ is plotted on the ordinate axis, with EW on the abscissa. Galaxy redshift is color-coded, with the colorbar to the right. The shaded region shows the parameter space that can be matched using the emergent line profile of a low- z galaxy (Hayes et al. 2023), when broadened synthetically to $\text{FWHM} = 500 \text{ km s}^{-1}$. We vary the IGM velocity out to 3000 km s^{-1} , and the EW between 0 and the very high value of 800\AA .

UV magnitudes. We show the distribution of these properties in Figure 1.

We note that this is a compilation of sources found in a number of different surveys, and its quantitative interpretation will be prone to selection effects. Nevertheless, there is a broad trend for galaxies with larger velocity shifts to show smaller EWs: this trend has been noted before, and is demonstrated in low- z samples (e.g. Hayes et al. 2023) where the IGM has no influence. The relation probably arises because more massive galaxies have higher column densities of neutral gas: Ly α photons must therefore undergo more scattering events in order to take longer frequency excursions to the wings of the line profile and see the gas as optically thin. This results in larger velocity offsets and also smaller Ly α escape fractions, because of the increased probability of dust absorption.

As the IGM gets thicker with increasing redshift, and ionized regions are presumably smaller, a trend of increasing $\Delta v_{\text{red}}(\text{Ly}\alpha)$ with redshift could be expected. However, the apparent trend for galaxies with larger velocity shifts to lie at $z \gtrsim 7.5$ is not found to be significant by a two-sample Kolmogorov-Smirnoff test.

3. MODELING GALAXIES AT REDSHIFT 6–11

3.1. The ‘Emergent’ Lyman alpha profile

We use three different adjectives to describe Ly α in this paper: the *intrinsic* values (profile and EW) that are produced by the H II regions, and the *observed* values are commonly used. Here we also use the term *emergent*, which refers to the

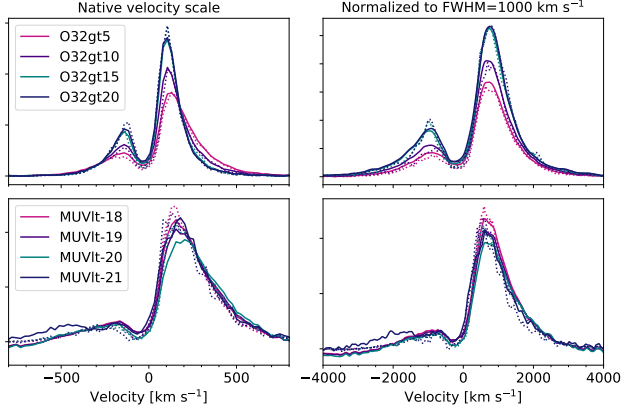


Figure 2. The emergent Ly α profiles. The left column shows the stacked profiles where each spectrum is simply renormalized by the Ly α luminosity at $\Delta v > 0$ prior to stacking. The upper-left panel shows how the profile varies when we select galaxies with successively higher O $_{32}$ ratios (above 5 in pink to above 20 in black). The lower left panels show the effect of stacking galaxies over different ranges of UV absolute magnitudes (less than -18 in pink to less than -21 in black). The right columns show the same as the left, but instead the spectra are also rescaled to the same FWHM of the red peak prior to stacking. The reference FWHM is arbitrarily set to 1000 km s^{-1} (note the different abscissa range). Solid lines are mean stacks and dotted lines are median.

Ly α emitted by the galaxy (after the CGM) but before attenuation by the IGM. The emergent Ly α profile is estimated from the sample of starburst galaxies at $0.05 < z < 0.44$ observed with the Cosmic Origins Spectrograph on HST (Hayes et al. 2021, 2023). At this redshift, the Ly α profile is unaffected by IGM absorption, and we showed in Hayes et al. (2021) that these profiles accurately reproduce those of Ly α -emitters at $3 \lesssim z \lesssim 6$ when the effects of an absorbing IGM are applied. Here we assert that the same general profile shape can be applied at higher redshifts still.

In Hayes et al. (2023) we produced stacked average Ly α spectra, where we binned the sample by various independent galaxy properties. Here we make use of the same software to simulate the emergent Ly α profiles from the EoR galaxies. We show some examples in Figure 2. We stack spectra based up measured quantities that match galaxies recently observed with JWST/NIRSpec (e.g. Brinchmann 2022; Cameron et al. 2023; Tang et al. 2023), such as high $[\text{O III}]\lambda 5007/[\text{O II}]\lambda 3727$ line ratios ($\equiv \text{O}_{32}$). Because we are interested most in the profile of the Ly α at velocities redwards of line-centre, we first renormalize our spectra by the redshifted luminosity prior to stacking. In the left panels we show how the profile varies when samples with successively higher O $_{32}$ ratios are taken (pink–purple–black). At higher O $_{32}$ the blue peak increases and the red peak narrows. The lower panel shows the same

but for increasingly luminous galaxies: in this case there is very little evolution in the emergent line profile.

In the right panel of the Figure 2 we show stacks of the same bins of galaxies as the left, but spectra are also normalized by the FWHM of the redshifted emission. Here we have re-scaled the spectra to FWHM= 1000 km s^{-1} which results in matched red wings. Our software can generate an emergent line profile for any FWHM, and treats FWHM as a free parameter.

3.2. Absorption by the Intergalactic Medium

With a model for the emergent Ly α profiles, we attenuate the spectra with a model intergalactic medium. We take the cosmic baryon density scaled by a factor of $(1 + z_{\text{sys}})^3$, and convert this into the hydrogen number density. From this we calculate the expected Ly α optical depth profile $\tau_{\text{IGM}}(v)$ as a function of velocity, as radiation redshifts through a neutral universe.

The unknown quantity is by how much the Ly α is cosmologically redshifted before it encounters the absorbing H I in the foreground. We estimate the absorption of Ly α using Voigt profiles, implementing successive absorptions numerically over velocity shift, Δv_{IGM} , which equates to a distance in an expanding universe. We multiply the emergent Ly α profile by $\exp(-\tau_{\text{IGM}}(v))$ and calculate the zeroth and first moments of the ‘observed’ profile. For a given emergent EW we rescale the zeroth moment to an ‘observed’ EW that accounts for the IGM. I.e $EW_{\text{obs}} = EW_{\text{emerge}}(m_{0,\text{obs}}/m_{0,\text{emerge}})$. EW_{emerge} therefore becomes a free parameter in our model, and can be compared with the EWs and velocity shifts shown in Figure 1.

3.3. Bayesian Inference on EW_{em} , $FWHM_{\text{red}}$, and R_{Bub}

For each galaxy, we perform a hierarchical Bayesian inference analysis to estimate the free parameters of our model: EW_{em} , $FWHM_{\text{red}}$, and R_{Bub} . We model the likelihood of observing the available data, i.e., the pair of $\{EW_{\text{obs}} \pm \sigma_{EW_{\text{obs}}}, \Delta(v_{\text{Ly}\alpha})_{\text{obs}} \pm \sigma_{\Delta(v_{\text{Ly}\alpha})}\}$, with a bivariate Normal distribution including known errors. Defining the vector of model parameters as $\theta = \{EW_{\text{em}}, FWHM_{\text{red}}, v_{\text{IGM}}\}$, we write the posterior for θ as:

$$p(\theta | EW_{\text{obs}}, \sigma_{EW_{\text{obs}}}, \Delta(v_{\text{Ly}\alpha})_{\text{obs}}, \sigma_{\Delta(v_{\text{Ly}\alpha})}, M_{\text{UV}}) \propto N(EW_{\text{tr}}, \Delta(v_{\text{Ly}\alpha})_{\text{tr}} | \sigma_{EW_{\text{obs}}}, \sigma_{\Delta(v_{\text{Ly}\alpha})}, \theta, M_{\text{UV}}) p(\theta | M_{\text{UV}})$$

where $p(\theta | M_{\text{UV}})$ is the prior on the model parameters, given the UV magnitude of each galaxy. Subscript ‘tr’ refers to Ly α quantities after transmission through the IGM, which are compared to the observed quantities given a subscript ‘obs’. We assume that $p(\theta | M_{\text{UV}}) = p(EW_{\text{em}})p(v_{\text{IGM}})p(FWHM_{\text{red}} | M_{\text{UV}})$, i.e., the priors on the emergent EW, the Ly α line width and the bubble radius are

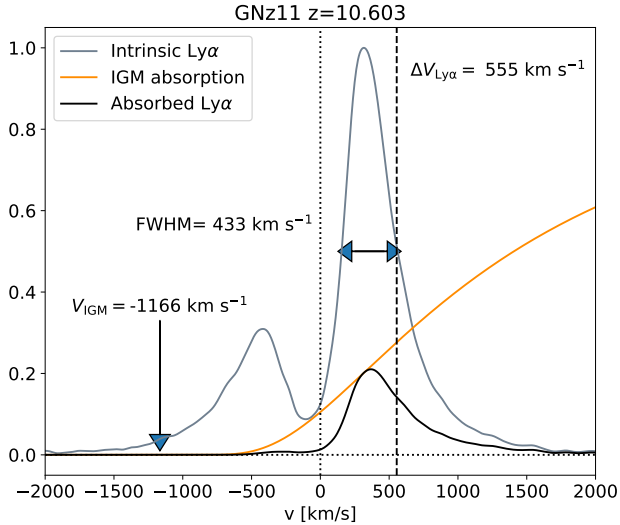


Figure 3. Example results for GNz11. We show the emergent Ly α profile as the grey line and the shape of the best-recovered Gunn Peterson absorption in orange. The observed Ly α profile is the product of the two and is shown in black. Various characteristic velocities are labeled.

independent. The prior on Δv_{IGM} is the simplest to treat – we have no empirical knowledge of this and adopt a uniform prior. For the emergent FWHM distribution we base our prior upon strong trends between M_{UV} and the FWHM of the red peak. We adopt measurements from the *Lyman alpha Spectral Database* (LASD; Runholm et al. 2021)¹ and the GALEX-measured UV magnitudes (see Hayes et al. 2023, Figure 21 of the online-only material) and fit a power-law between FWHM and M_{UV} ; our prior is then Normal around this relation, and includes errors on the fit. For the emergent Ly α EW we adopt an exponential distribution based upon the very deep MUSE observations of Hashimoto et al. (2017). We take the scale length estimated at $z = 6$ corrected for absorption by the IGM ($EW_0 = 212 \pm 186 \text{ \AA}$), making the assumption that the EW distribution does not evolve strongly over the redshift of the sample.

We sample the posterior distribution using a Metropolis Hastings sampler built in PYCM (Salvatier et al. 2016). Δv_{IGM} is converted to R_{Bub} after the fact using Hubble’s law. We show an example fit in Figure 3. In Figure 4 we show the posterior distribution functions for EW_{em} , $FWHM_{\text{red}}$, and R_{bubble} for each galaxy (light curves) and for three samples, divided according to redshift. In the discussion that follows, we use the maximum a posteriori and its associated 68% credibility interval as our best estimate and associated uncertainty on each parameter.

¹ <http://lasd.lyman-alpha.com>

4. MAIN RESULTS AND DISCUSSION

4.1. An Example: GNz11

We show an example profile for GNz11 (Bunker et al. 2023) in Figure 3. This is currently the highest redshift known Ly α -emitting galaxy. The galaxy has an observed Ly α EW of 18 \AA , and $\Delta v_{\text{red}}(\text{Ly}\alpha)$ of 555 km s^{-1} . While it may be an AGN, our models show that its spectral properties in Ly α can be recovered with relatively normal conditions. Naively, it may be considered difficult to explain a Ly α emission line from $z \approx 11$, but in actually it is not especially hard.

The maximum of the posterior on the Ly α FWHM is 433 km s^{-1} – this is high for a galaxy, indeed, and the highest we find in the $z \sim 0$ COS sample has a FWHM in the red peak of only 350 km s^{-1} . Nevertheless, 433 km s^{-1} is not so much higher that we consider it unrealistic. This modeled broad Ly α has a wing visible out to $v \approx 1500 \text{ km s}^{-1}$ at low flux density. The maximum of the posterior probability function for the IGM velocity is almost 1200 km s^{-1} – at this velocity offset, the damping wing draws a steep diagonal line across the emerging red Ly α peak, absorbing ~ 4 times as much flux at $v = 0$ compared to at 1000 km s^{-1} . The result is a significant shift in the first moment of the line, to the 555 km s^{-1} that is observed. In doing so the Ly α is also significantly suppressed, and only $\sim 7\%$ of the emergent Ly α survives IGM absorption. The emergent Ly α EW is $\approx 260 \text{ \AA}$ with a credibility range of $153\text{--}800 \text{ \AA}$ at $16\text{--}84\%$. This value is again high for a star-forming galaxy, but not higher than observed in galaxies at effectively all redshifts. Based upon the observed H γ flux and Case B recombination theory, Bunker et al. (2023) estimate that around 4% of the *intrinsic* Ly α escapes the galaxy. This is comparable to the 7% we estimate from the *emergent* Ly α flux; the further factor of ~ 2 could indicate that $\sim 50\%$ of the intrinsic Ly α escapes the galaxy after internal radiative transfer effects.

4.2. Sample-Averaged Galaxy Properties

We take the H I velocity offsets, emergent Ly α EW and FWHM from the maximum values of the posterior sampling as described in Section 3.3. Emergent EWs are typically peaked towards the lower end of the distribution near 100 \AA – a value that is quite typical of star-forming galaxies and does not require extreme stellar populations or AGN. Only a handful of individual galaxies show posteriors that peak at EWs above 200 \AA , one of which is obviously JADES-GS-z7-LA, with its observed EW of 400 \AA .

The FWHM also peak in ranges that are typical of star forming galaxies at low- z , of around 200 km s^{-1} , with a tail up to 600 km s^{-1} . Here there is a more obvious signature for galaxies at the higher redshifts to be intrinsically broader than those at $z = 6\text{--}8.5$, although we note that this highest redshift bin contains only three galaxies. This may be a signature of a selection bias in the requirement of Ly α , where only broad

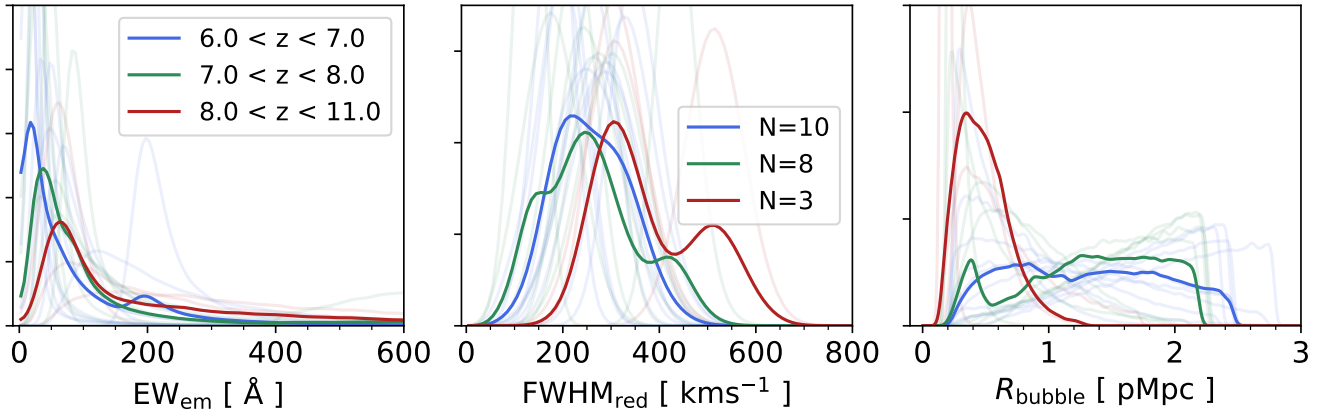


Figure 4. Binned probability distribution functions from traces of the Monte Carlo sampler. Left shows the emergent Ly α EW, and centre shows the FWHM of the Ly α red peak. Right shows the bubble size in proper Mpc. Each posterior is color-coded by redshift, as labeled in the left plot. Hard lines show the binned products of the posterior distributions, while faint lines show those for individual galaxies. The number of galaxies per bin is shown in the legend of the central plot.

emergent Ly α profiles are able evade the damping wing of the IGM and be reported as a Ly α detection.

4.3. The Sizes of Ionized Regions – Evolution Through the EoR

After converting the IGM velocity offset to a foreground H I distance using the Hubble parameter, we show the resulting combined posterior probabilities in the right panel of Figure 4. Estimated H I foreground distances generally show flat posteriors for the $z = 6 - 8$ subsamples, with distances just below a Mpc and extend to 3-4 Mpc. However the combined posterior of the $z > 8$ subsample is much more strongly peaked around distances below 1 pMpc, shows a much sharper decline with redshift, and drops to zero at 2 pMpc.

In Figure 5 we show the evolution of the distance to the foreground screen of H I (taking the peak of the posterior) as a function of redshift. Distances to the foreground H I screen range from around 1 to 3 proper Mpc at the lower redshift end. We note that our approach – and observations in general – may not be sensitive to smaller bubble radii, as a certain minimum offset will be required for Ly α to be detected, and therefore be reported in the literature with a velocity shift. There is in principle no reason why the method could not be applied to galaxies without Ly α emission, but in order to avoid great degeneracies such an approach would require more informed priors on the intrinsic EW. This could perhaps be attained from optical line emission (e.g. Runnholm et al. 2020; Hayes et al. 2023).

The interpretation of the larger radii at $z \approx 6$ is likely to be that these galaxies reside in an ionized universe, and far out in the damping wing (after $\sim 2000 \text{ km s}^{-1}$) there is little power in the IGM to modulate the Ly α observables – the method breaks down for large bubbles and all Δv_{IGM} are equally valid.

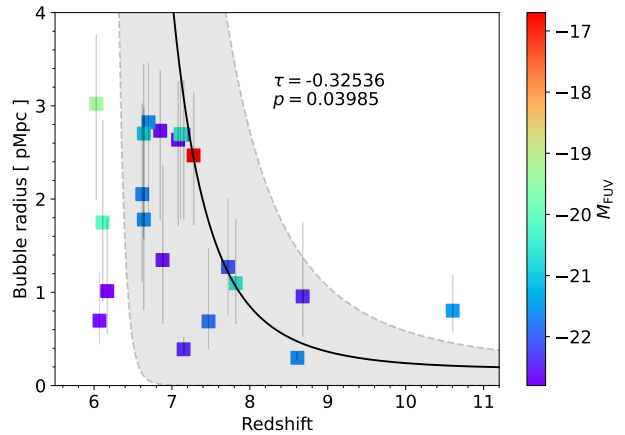


Figure 5. Evolution of the bubble radius, R_{Bub} (ordinate) with redshift (abscissa). Uncertainties refer to the 16th and 84th percentiles of the posterior. Absolute UV magnitude is color-coded. The shaded regions shows the 10-90-percentile range of bubble sizes from the simulation of Giri & Mellema (2021).

The lower end of the distribution ($\Delta v_{\text{IGM}} \approx 1 \text{ pMpc}$) are consistent estimates from Ly α spectral profiles (Mason & Gronke 2020) and from ionization balance considerations (Bagley et al. 2017), both of which are estimated at comparable redshifts.

Figure 5 is striking in its absence of larger bubbles at higher redshifts. Using Kendall's τ statistic, we find the trend to be significant at $p = 3.9 \times 10^{-2}$. If taken at face value, the result implies that ionized regions increase in size from $z \approx 11$ to $z \approx 6$ – this empirical find of ionized regions growing with time fulfills the main expectations of reionization.

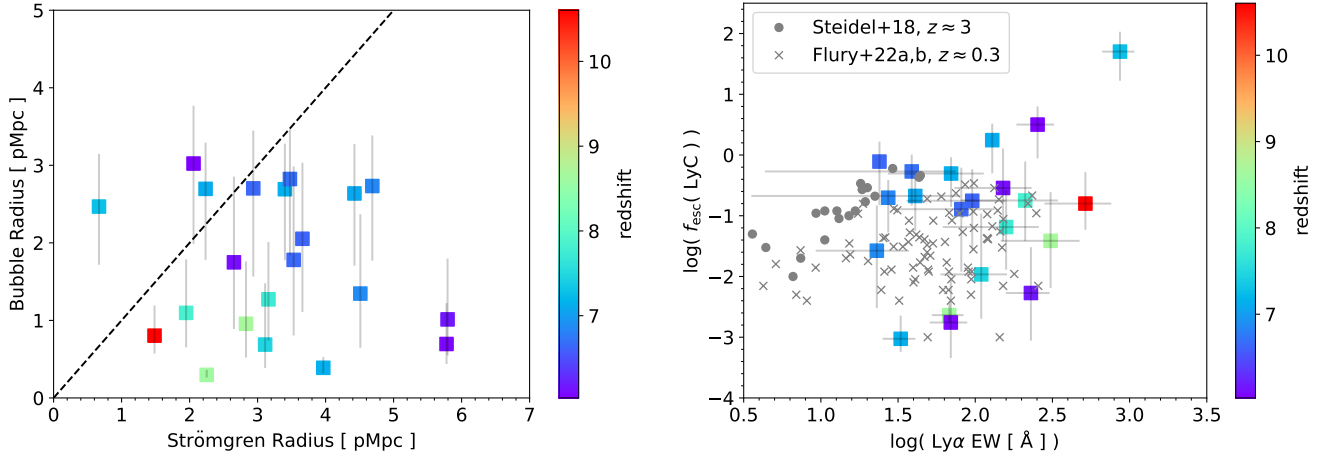


Figure 6. Left: the radii of the bubble inferred from Ly α modeling (R_{Bub}), contrasted with that of the Strömgren sphere (R_{Strom}). Right: the comparison of the LyC escape fraction ($f_{\text{esc}}^{\text{LyC}}$; inferred from the left plot) with the model-inferred EW of Ly α . We over-plot the values measured at $z \approx 3$ by Steidel et al. (2018) and at $z \approx 0.3$ by Flury et al. (2022a). Redshift is color-coded in both cases.

In the same figure we also show computational results from Giri & Mellema (2021). The simulated relation takes a similar qualitative form, rising sharply across the redshift range. However, it rises much faster than our data suggest, evolving into a fully ionized universe (effectively infinite bubble radii) by $z \approx 6.5$. There are four observed galaxies at $z \sim 6$ that seemingly have much smaller bubble radii than suggested by the simulations. If the universe is fully ionized by $z = 6$, these could be the result of proximate Ly α -absorbing systems (possibly galaxies) whose damping wings redshift the Ly α and cause our model estimate smaller radii. This result may reflect the high end of the broad range of Ly α optical depths observed in quasar spectra at $z \approx 6$ (e.g. Bosman et al. 2022).

At the other end of the redshift range, GNz11 at $z = 10.6$ shows a far larger bubble radius than expected from the simulations, which is harder to explain. From the simulation volume of $3.6 \times 10^8 \text{ cMpc}^3$ and recent estimates of the galaxy luminosity function at this redshift (Donnan et al. 2023), we expect there to be several hundred galaxies like GNz11 in the simulation volume. This currently represents a tension that could be resolved in several ways. Observationally, the EW or velocity offset may be impacted by systematic uncertainties such as spectroscopic aperture corrections or intrinsic asymmetry in the Ly α profile that skews the centroid of the emission line. In our model, the restrictive prior on the EW distribution or FWHM– M_{FUV} relation may skew the bubble radius to artificially high values. Finally the simulation setup may not accurately capture the diversity of bubble sizes at the highest redshifts, especially as JWST is now identifying numbers of galaxies at this epoch that exceed the expectations when the simulation was run.

4.4. The Escape of Ionizing Radiation

We showed above that we can estimate the distance between the galaxy and the absorbing H I gas in the foreground. Each galaxy is likely highly star-forming, as evidenced by the relatively strong Ly α emission (emergent EWs of 100 Å, with intrinsic values likely much higher still). Adopting the estimated ionizing photon production efficiency for GNz11 of $5.2 \times 10^{25} \text{ Hz erg}^{-1}$ (Bunker et al. 2023) we convert the measured far UV luminosity to an intrinsic rate of ionizing photon production. Using the cosmic number density of hydrogen atoms used for the Gunn Peterson calculation (Section 3.2), we also solve the equation for the radius of the Strömgren sphere. We derive values between 0.5 and 6 Mpc, which we contrast with 1–3 Mpc for the distance to the foreground H I in the left panel of Figure 6.

If we assume that each reported galaxy is singularly responsible for ionizing the region around it, that it lies at the centre of its bubble and has an ionizing escape fraction ($f_{\text{esc}}^{\text{LyC}}$) of one, these numbers would be equivalent. Of course this last point is not true, as ionizing photons are required to make the Ly α . The escape fraction of ionizing photons is not known and cannot be measured at this redshift. However, Under the assumptions stated above we can compute $f_{\text{esc}}^{\text{LyC}}$ from the ratio of above distances: $f_{\text{esc}}^{\text{LyC}} = (R_{\text{Bub}}/R_{\text{Strom}})^3$. For GNz11 we estimate $f_{\text{esc}}^{\text{LyC}}$ to be 16 % with a 1σ confidence range of 6-50%. This is just coincident with the upper end of that estimated by Bunker et al. (2023), which is $0.03_0^{0.05}$.

This gives a median value of $f_{\text{esc}}^{\text{LyC}} = 17 \%$, with a 16–84 percentile range of 6–72%. We show the inferred $f_{\text{esc}}^{\text{LyC}}$ against the model inferred EW of Ly α in the right panel of Figure 6. These two quantities are strongly correlated at low- and mid-redshifts and we overplot the individual data points of Flury et al. (2022b) and stacks and Steidel et al. (2018) for comparison. Our estimates clearly span the same range

as the lower redshift estimates. While this plot is suggestive that relationship could also be identifiable for galaxies in the EoR, we do not yet have sufficient samples to make similar statements.

One galaxy has $f_{\text{esc}}^{\text{LyC}} > 1$ and significantly outliers from the distribution, with an apparent $f_{\text{esc}}^{\text{LyC}}$ of 100 when the modeling finds a distance to the foreground H I that is larger than the Strömgen radius. This is the extreme galaxy GS-z7-LA (Saxena et al. 2023), with Ly α EW of 400Å. It may be a result of the modeling finding too large bubbles when it cannot find strong evidence of a GP absorption (little redshift of Ly α and high EWs). It could also be explained if there are a number of galaxies in the bubble and we do not identify the main contributor(s) – we suggest this is likely the case for GS-z7-LA.

5. CONCLUDING REMARKS

We have built a hierarchical Bayesian model to estimate the intrinsic Ly α observables (emergent equivalent width and kinematic offset from systemic velocity) of galaxies in the reionization epoch, as well as the size of the ionized regions (‘bubbles’) in which they must reside. The model is built upon empirical Ly α spectral templates observed in lower redshift galaxies where the IGM has no impact, and estimates the IGM absorption at a given redshift that best matches observation. We have applied this framework to a sample of 21 ostensibly star-forming galaxies at redshift $z \approx 6 - 11$ where systemic redshifts are available, including very recent observations from JWST. We find the following main results.

- The observed galaxies occupy ionized regions with sizes between 0.5 and 3 proper Mpc. The posterior probability distribution of the bubble size is not invariant with redshift, and is skewed towards smaller bubbles at higher redshifts. We detect an upwards evolution of the bubble size with redshift that is significant at better than 3σ and demonstrates that ionized regions grow with time. The recovered bubble radii are broadly consistent with results from numerical simulations of reionization.
- From the observed UV luminosity and reported ionizing photon production efficiencies, we compute the size of the Strömgen radius of each galaxy under the assumption of photoionization equilibrium. The Strömgen radius does not correlate with the bubble radius. We use the ratio of these two radii to estimate the escape fraction of ionizing photons, recovering a median value of 17% – this is consistent with the requirements for galaxies to reionize the universe. Our estimates of $f_{\text{esc}}^{\text{LyC}}$ and Ly α EW are comparable to those derived at lower- z , but we do not yet recover the correlation between these quantities.

ACKNOWLEDGEMENTS

We thank Sambit Giri, Ivelin Georgiev and Garrelt Mellema for making simulation data available for Figure 5. We also thank Axel Runnholm and Max Gronke for useful discussions and further ongoing contributions to the projects. M.H. acknowledges the support of the Swedish Research Council, Vetenskapsrådet and is Fellow of the Knut and Alice Wallenberg Foundation.

REFERENCES

- Arrabal Haro, P., Rodríguez Espinosa, J. M., Muñoz-Tuñón, C., et al. 2018, MNRAS, 478, 3740, doi: [10.1093/mnras/sty1106](https://doi.org/10.1093/mnras/sty1106)
- Bagley, M. B., Scarlata, C., Henry, A., et al. 2017, ApJ, 837, 11, doi: [10.3847/1538-4357/837/1/11](https://doi.org/10.3847/1538-4357/837/1/11)
- Bosman, S. E. I., Davies, F. B., Becker, G. D., et al. 2022, MNRAS, 514, 55, doi: [10.1093/mnras/stac1046](https://doi.org/10.1093/mnras/stac1046)
- Brinchmann, J. 2022, arXiv e-prints, arXiv:2208.07467, doi: [10.48550/arXiv.2208.07467](https://doi.org/10.48550/arXiv.2208.07467)
- Bunker, A. J., Saxena, A., Cameron, A. J., et al. 2023, arXiv e-prints, arXiv:2302.07256, doi: [10.48550/arXiv.2302.07256](https://doi.org/10.48550/arXiv.2302.07256)
- Cameron, A. J., Saxena, A., Bunker, A. J., et al. 2023, arXiv e-prints, arXiv:2302.04298, doi: [10.48550/arXiv.2302.04298](https://doi.org/10.48550/arXiv.2302.04298)
- Carniani, S., Maiolino, R., Pallottini, A., et al. 2017, A&A, 605, A42, doi: [10.1051/0004-6361/201630366](https://doi.org/10.1051/0004-6361/201630366)
- Cassata, P., Tasca, L. A. M., Le Fèvre, O., et al. 2015, A&A, 573, A24, doi: [10.1051/0004-6361/201423824](https://doi.org/10.1051/0004-6361/201423824)
- Dijkstra, M. 2014, PASA, 31, e040, doi: [10.1017/pasa.2014.33](https://doi.org/10.1017/pasa.2014.33)
- Dijkstra, M., Haiman, Z., & Spaans, M. 2006, ApJ, 649, 14, doi: [10.1086/506243](https://doi.org/10.1086/506243)
- Dijkstra, M., Wyithe, J. S. B., & Haiman, Z. 2007, MNRAS, 379, 253, doi: [10.1111/j.1365-2966.2007.11936.x](https://doi.org/10.1111/j.1365-2966.2007.11936.x)
- Donnan, C. T., McLeod, D. J., Dunlop, J. S., et al. 2023, MNRAS, 518, 6011, doi: [10.1093/mnras/stac3472](https://doi.org/10.1093/mnras/stac3472)
- Endsley, R., Stark, D. P., Bouwens, R. J., et al. 2022, MNRAS, 517, 5642, doi: [10.1093/mnras/stac3064](https://doi.org/10.1093/mnras/stac3064)
- Finkelstein, S. L., Bagley, M. B., Arrabal Haro, P., et al. 2022, ApJL, 940, L55, doi: [10.3847/2041-8213/ac966e](https://doi.org/10.3847/2041-8213/ac966e)
- Flury, S. R., Jaskot, A. E., Ferguson, H. C., et al. 2022a, ApJS, 260, 1, doi: [10.3847/1538-4365/ac5331](https://doi.org/10.3847/1538-4365/ac5331)
- . 2022b, ApJ, 930, 126, doi: [10.3847/1538-4357/ac61e4](https://doi.org/10.3847/1538-4357/ac61e4)
- Giri, S. K., & Mellema, G. 2021, MNRAS, 505, 1863, doi: [10.1093/mnras/stab1320](https://doi.org/10.1093/mnras/stab1320)
- Hashimoto, T., Garel, T., Guiderdoni, B., et al. 2017, A&A, 608, A10, doi: [10.1051/0004-6361/201731579](https://doi.org/10.1051/0004-6361/201731579)

- Hayes, M., Schaerer, D., Östlin, G., et al. 2011, *ApJ*, 730, 8, doi: [10.1088/0004-637X/730/1/8](https://doi.org/10.1088/0004-637X/730/1/8)
- Hayes, M. J., Runnholm, A., Gronke, M., & Scarlata, C. 2021, *ApJ*, 908, 36, doi: [10.3847/1538-4357/abd246](https://doi.org/10.3847/1538-4357/abd246)
- Hayes, M. J., Runnholm, A., Scarlata, C., Gronke, M., & Rivera-Thorsen, T. E. 2023, *MNRAS*, doi: [10.1093/mnras/stad477](https://doi.org/10.1093/mnras/stad477)
- Kashikawa, N., Shimasaku, K., Malkan, M. A., et al. 2006, *ApJ*, 648, 7, doi: [10.1086/504966](https://doi.org/10.1086/504966)
- Laursen, P., Sommer-Larsen, J., & Andersen, A. C. 2009, *ApJ*, 704, 1640, doi: [10.1088/0004-637X/704/2/1640](https://doi.org/10.1088/0004-637X/704/2/1640)
- Mainali, R., Kollmeier, J. A., Stark, D. P., et al. 2017, *ApJL*, 836, L14, doi: [10.3847/2041-8213/836/1/L14](https://doi.org/10.3847/2041-8213/836/1/L14)
- Malhotra, S., & Rhoads, J. E. 2004, *ApJL*, 617, L5, doi: [10.1086/427182](https://doi.org/10.1086/427182)
- Mason, C. A., & Gronke, M. 2020, *MNRAS*, 499, 1395, doi: [10.1093/mnras/staa2910](https://doi.org/10.1093/mnras/staa2910)
- Mason, C. A., Treu, T., Dijkstra, M., et al. 2018, *ApJ*, 856, 2, doi: [10.3847/1538-4357/aab0a7](https://doi.org/10.3847/1538-4357/aab0a7)
- Matthee, J., Sobral, D., Gronke, M., et al. 2018, *A&A*, 619, A136, doi: [10.1051/0004-6361/201833528](https://doi.org/10.1051/0004-6361/201833528)
- Miralda-Escudé, J., & Rees, M. J. 1998, *ApJ*, 497, 21, doi: [10.1086/305458](https://doi.org/10.1086/305458)
- Pentericci, L., Carniani, S., Castellano, M., et al. 2016, *ApJL*, 829, L11, doi: [10.3847/2041-8205/829/1/L11](https://doi.org/10.3847/2041-8205/829/1/L11)
- Runnholm, A., Gronke, M., & Hayes, M. 2021, *PASP*, 133, 034507, doi: [10.1088/1538-3873/abe3ca](https://doi.org/10.1088/1538-3873/abe3ca)
- Runnholm, A., Hayes, M., Melinder, J., et al. 2020, *ApJ*, 892, 48, doi: [10.3847/1538-4357/ab7a91](https://doi.org/10.3847/1538-4357/ab7a91)
- Salvatier, J., Wiecki, T. V., & Fonnesbeck, C. 2016, *PeerJ Computer Science*, 2, e55, doi: [10.7717/peerj-cs.55](https://doi.org/10.7717/peerj-cs.55)
- Saxena, A., Robertson, B. E., Bunker, A. J., et al. 2023, arXiv e-prints, arXiv:2302.12805, doi: [10.48550/arXiv.2302.12805](https://doi.org/10.48550/arXiv.2302.12805)
- Schenker, M. A., Ellis, R. S., Konidaris, N. P., & Stark, D. P. 2014, *ApJ*, 795, 20, doi: [10.1088/0004-637X/795/1/20](https://doi.org/10.1088/0004-637X/795/1/20)
- Stark, D. P., Ellis, R. S., & Ouchi, M. 2011, *ApJL*, 728, L2, doi: [10.1088/2041-8205/728/1/L2](https://doi.org/10.1088/2041-8205/728/1/L2)
- Stark, D. P., Richard, J., Charlot, S., et al. 2015, *MNRAS*, 450, 1846, doi: [10.1093/mnras/stv688](https://doi.org/10.1093/mnras/stv688)
- Stark, D. P., Ellis, R. S., Charlot, S., et al. 2017, *MNRAS*, 464, 469, doi: [10.1093/mnras/stw2233](https://doi.org/10.1093/mnras/stw2233)
- Steidel, C. C., Bogosavljević, M., Shapley, A. E., et al. 2018, *ApJ*, 869, 123, doi: [10.3847/1538-4357/aaed28](https://doi.org/10.3847/1538-4357/aaed28)
- Tang, M., Stark, D. P., Chen, Z., et al. 2023, arXiv e-prints, arXiv:2301.07072, doi: [10.48550/arXiv.2301.07072](https://doi.org/10.48550/arXiv.2301.07072)
- Verhamme, A., Schaerer, D., & Maselli, A. 2006, *A&A*, 460, 397, doi: [10.1051/0004-6361:20065554](https://doi.org/10.1051/0004-6361:20065554)
- Wold, I. G. B., Finkelstein, S. L., Barger, A. J., Cowie, L. L., & Rosenwasser, B. 2017, *ApJ*, 848, 108, doi: [10.3847/1538-4357/aa8d6b](https://doi.org/10.3847/1538-4357/aa8d6b)